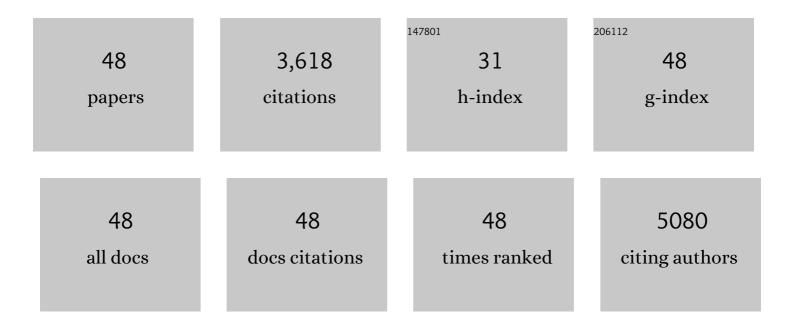
Dawen Zeng

List of Publications by Year in descending order

Source: https://exaly.com/author-pdf/2612156/publications.pdf Version: 2024-02-01



DAMEN ZENC

#	Article	IF	CITATIONS
1	Enhanced Photocatalytic Activity of Chemically Bonded TiO ₂ /Graphene Composites Based on the Effective Interfacial Charge Transfer through the C–Ti Bond. ACS Catalysis, 2013, 3, 1477-1485.	11.2	461
2	Metal-oxide-semiconductor based gas sensors: screening, preparation, and integration. Physical Chemistry Chemical Physics, 2017, 19, 6313-6329.	2.8	400
3	In situ synthesis of C-TiO2/g-C3N4 heterojunction nanocomposite as highly visible light active photocatalyst originated from effective interfacial charge transfer. Applied Catalysis B: Environmental, 2017, 202, 489-499.	20.2	262
4	Interface Bonds Determined Gas-Sensing of SnO ₂ –SnS ₂ Hybrids to Ammonia at Room Temperature. ACS Applied Materials & Interfaces, 2015, 7, 11359-11368.	8.0	191
5	Multilevel Microstructured Flexible Pressure Sensors with Ultrahigh Sensitivity and Ultrawide Pressure Range for Versatile Electronic Skins. Small, 2019, 15, e1804559.	10.0	163
6	Enhanced room-temperature NH3 gas sensing by 2D SnS2 with sulfur vacancies synthesized by chemical exfoliation. Sensors and Actuators B: Chemical, 2018, 262, 771-779.	7.8	140
7	Pore size dependent gas-sensing selectivity based on ZnO@ZIF nanorod arrays. Sensors and Actuators B: Chemical, 2018, 258, 1099-1106.	7.8	134
8	2D WS2 nanosheets with TiO2 quantum dots decoration for high-performance ammonia gas sensing at room temperature. Sensors and Actuators B: Chemical, 2017, 253, 1034-1042.	7.8	128
9	Al-doping induced formation of oxygen-vacancy for enhancing gas-sensing properties of SnO2 NTs by electrospinning. Sensors and Actuators B: Chemical, 2014, 198, 62-69.	7.8	107
10	Effect of layer number on recovery rate of WS 2 nanosheets for ammonia detection at room temperature. Applied Surface Science, 2017, 414, 244-250.	6.1	107
11	Selectively enhanced UV and NIR photoluminescence from a degenerate ZnO nanorod array film. Journal of Materials Chemistry C, 2014, 2, 4566.	5.5	104
12	ZnO Micro/Nanocrystals with Tunable Exposed (0001) Facets for Enhanced Catalytic Activity on the Thermal Decomposition of Ammonium Perchlorate. Journal of Physical Chemistry C, 2014, 118, 11833-11841.	3.1	95
13	Graphene-wrapped WO3 nanospheres with room-temperature NO2 sensing induced by interface charge transfer. Sensors and Actuators B: Chemical, 2015, 220, 201-209.	7.8	91
14	Hierarchical porous SnO2 micro-rods topologically transferred from tin oxalate for fast response sensors to trace formaldehyde. Sensors and Actuators B: Chemical, 2014, 190, 585-592.	7.8	87
15	La2O3-sensitized SnO2 nanocrystalline porous film gas sensors and sensing mechanism toward formaldehyde. Sensors and Actuators B: Chemical, 2013, 188, 137-146.	7.8	70
16	A facile low-temperature synthesis of hierarchical porous Co ₃ O ₄ micro/nano structures derived from ZIF-67 assisted by ammonium perchlorate. Inorganic Chemistry Frontiers, 2019, 6, 715-722.	6.0	68
17	Pore-size-dependent sensing property of hierarchical SnO2 mesoporous microfibers as formaldehyde sensors. Sensors and Actuators B: Chemical, 2013, 186, 640-647.	7.8	64
18	Room temperature NO ₂ sensing: what advantage does the rGO–NiO nanocomposite have over pristine NiO?. Physical Chemistry Chemical Physics, 2015, 17, 14903-14911.	2.8	59

DAWEN ZENG

#	Article	IF	CITATIONS
19	Mechanisms and Applications of Steady-State Photoluminescence Spectroscopy in Two-Dimensional Transition-Metal Dichalcogenides. ACS Nano, 2020, 14, 14579-14604.	14.6	56
20	A review on two-dimensional materials for chemiresistive- and FET-type gas sensors. Physical Chemistry Chemical Physics, 2021, 23, 15420-15439.	2.8	49
21	Enhanced room temperature NO ₂ response of NiO–SnO ₂ nanocomposites induced by interface bonds at the p–n heterojunction. Physical Chemistry Chemical Physics, 2016, 18, 5386-5396.	2.8	47
22	Catalytic Activation of Cobalt Doping Sites in ZIF-71-Coated ZnO Nanorod Arrays for Enhancing Gas-Sensing Performance to Acetone. ACS Applied Materials & Interfaces, 2020, 12, 48948-48956.	8.0	47
23	An In2O3 nanowire-like network fabricated on coplanar sensor surface by sacrificial CNTs for enhanced gas sensing performance. Sensors and Actuators B: Chemical, 2013, 185, 345-353.	7.8	46
24	The atomic origin of high catalytic activity of ZnO nanotetrapods for decomposition of ammonium perchlorate. CrystEngComm, 2014, 16, 570-574.	2.6	43
25	A new approach for an ultrasensitive tactile sensor covering an ultrawide pressure range based on the hierarchical pressure-peak effect. Nanoscale Horizons, 2020, 5, 541-552.	8.0	41
26	Gas Adsorption at Metal Sites for Enhancing Gas Sensing Performance of ZnO@ZIF-71 Nanorod Arrays. Langmuir, 2019, 35, 3248-3255.	3.5	40
27	Vanadium-Doped Monolayer MoS ₂ with Tunable Optical Properties for Field-Effect Transistors. ACS Applied Nano Materials, 2021, 4, 769-777.	5.0	39
28	A novel approach to fabricate metal oxide nanowire-like networks based coplanar gas sensors array for enhanced selectivity. Sensors and Actuators B: Chemical, 2014, 204, 351-359.	7.8	38
29	Two-Dimensional Hexagonal Boron Nitride for Building Next-Generation Energy-Efficient Devices. ACS Energy Letters, 2021, 6, 985-996.	17.4	37
30	Enhanced visible-light photocatalytic performance of highly-dispersed Pt/g-C ₃ N ₄ nanocomposites by one-step solvothermal treatment. RSC Advances, 2017, 7, 33552-33557.	3.6	36
31	Quantifying Quasiâ€Fermi Level Splitting and Mapping its Heterogeneity in Atomically Thin Transition Metal Dichalcogenides. Advanced Materials, 2019, 31, e1900522.	21.0	34
32	Enhanced response to NO2 with CuO/ZnO laminated heterostructured configuration. Sensors and Actuators B: Chemical, 2014, 195, 500-508.	7.8	33
33	Modulated interlayer charge transfer dynamics in a monolayer TMD/metal junction. Nanoscale, 2019, 11, 418-425.	5.6	33
34	High-Adhesion Stretchable Electrode via Cross-Linking Intensified Electroless Deposition on a Biomimetic Elastomeric Micropore Film. ACS Applied Materials & Interfaces, 2019, 11, 20535-20544.	8.0	33
35	2D organic single crystals: Synthesis, novel physics, high-performance optoelectronic devices and integration. Materials Today, 2021, 50, 442-475.	14.2	32
36	Characterization of Photoelectric Properties and Composition Effect of TiO ₂ /ZnO/Fe ₂ O ₃ Composite by Combinatorial Methodology. ACS Combinatorial Science, 2010, 12, 883-889.	3.3	31

Dawen Zeng

#	Article	IF	CITATIONS
37	Processing–microstructure–property correlations of gas sensors based on ZnO nanotetrapods. Sensors and Actuators B: Chemical, 2013, 181, 509-517.	7.8	28
38	Hierarchical ZnO hollow microspheres with exposed (001) facets as promising catalysts for the the the the the thermal decomposition of ammonium perchlorate. CrystEngComm, 2015, 17, 8689-8696.	2.6	26
39	Emission Control from Transition Metal Dichalcogenide Monolayers by Aggregation-Induced Molecular Rotors. ACS Nano, 2020, 14, 7444-7453.	14.6	23
40	Twist-driven wide freedom of indirect interlayer exciton emission in MoS2/WS2 heterobilayers. Cell Reports Physical Science, 2021, 2, 100509.	5.6	23
41	Origin of the efficient catalytic thermal decomposition of ammonium perchlorate over (2â^'1â^'10) facets of ZnO nanosheets: surface lattice oxygen. RSC Advances, 2017, 7, 40262-40269.	3.6	18
42	Aluminium and zinc co-doped CuInS2 QDs for enhanced trion modulation in monolayer WS2 toward improved electrical properties. Journal of Materials Chemistry C, 2019, 7, 15074-15081.	5.5	12
43	Temperature-Programmed Technique Accompanied with High-Throughput Methodology for Rapidly Searching the Optimal Operating Temperature of MOX Gas Sensors. ACS Combinatorial Science, 2014, 16, 459-465.	3.8	11
44	Synthesis of a novel N H TiO 2 photocatalyst by annealing in NH 3 and H 2 for complete decomposition of high concentration benzene under visible light irradiation. Materials Letters, 2014, 136, 258-261.	2.6	10
45	Mechanistic study of N–H- and H–N-codoping of a TiO ₂ photocatalyst for efficient degradation of benzene under visible light. RSC Advances, 2020, 10, 2757-2766.	3.6	10
46	Molecular sieving property adjusted by the encapsulation of Ag nanoparticles into ZnO@ZIF-71 nanorod arrays. Chemical Communications, 2019, 55, 11045-11048.	4.1	7
47	Solar Cells: Quantifying Quasiâ€Fermi Level Splitting and Mapping its Heterogeneity in Atomically Thin Transition Metal Dichalcogenides (Adv. Mater. 25/2019). Advanced Materials, 2019, 31, 1970180.	21.0	2
48	Interfacing transition metal dichalcogenides with chromium germanium telluride quantum dots for controllable light-matter interactions. Journal of Colloid and Interface Science, 2022, 611, 432-440.	9.4	2